Hindawi Publishing Corporation
Mathematical Problems in Engineering
Volume 2013, Article ID 532814, 11 pages
http://dx.doi.org/10.1155/2013/532814

Research Article

Estimation of Bottom Friction Coefficients Based on an Isopycnic-Coordinate Internal Tidal Model with Adjoint Method

Yanqiu Gao,[1] Anzhou Cao,[1] Haibo Chen,[1,2] and Xianqing Lv[1]

[1] *Laboratory of Physical Oceanography, Ocean University of China, Qingdao 266100, China*
[2] *China Offshore Environmental Services Ltd., Qingdao 266061, China*

Correspondence should be addressed to Haibo Chen; chenhb_2012@163.com

Received 16 September 2013; Revised 27 November 2013; Accepted 8 December 2013

Academic Editor: Franklin Mendivil

Based on an isopycnic-coordinate internal tidal model with the adjoint method, three groups of ideal experiments are carried out in order to investigate the estimation of spatially varying bottom friction coefficients (BFCs). In group 1, five values of distance between independent points (DIP) are used to invert the BFCs with the distribution of conical surface. Results show that the BFCs can be inverted successfully with independent point scheme and the strategy with a DIP of $50'$ can yield the best results. In group 2, five values of interpolation radius (IR) are used to invert the BFCs with the distribution of conical surface. Results show that the strategy with an IR of 1.9 times of DIP can yield the best results. Based on the results of the first two groups, group 3 adopts the optimal DIP and IR to estimate 4 kinds of spatially varying BFCs. The results indicate that the isopycnic-coordinate internal tidal model with the adjoint method has a good ability to estimate the spatially varying BFCs; the inversion results of the BFCs with the distribution of revolution paraboloid are better than those with the distribution of conical surface.

1. Introduction

Internal tides are internal waves with tidal frequency and generated in a stratified ocean as the barotropic tidal currents interact with topography [1–3]. They are ubiquitous in the oceans and play an important role in the dissipation of barotropic tides and in mixing the deep ocean [4–8]. Generally speaking, internal tides are mainly studied by analytical and numerical modeling because the in situ observations are rare. Rattray Jr. [9], Baines [10, 11], Gerkema [12], Garrett and Gerkema [13], Llewellyn Smith and Young [14], and Balmforth and Peacock [15] constructed analytical models and obtained the analytical solutions on ideal topographies so as to investigate the generation and propagation of internal tides. Although these analytical models aided us in understanding the tide-topography interaction process, they had to face some mathematical difficulties. Fortunately, numerical simulation has been able to provide us with an effective mean to study internal tides. Chuang and Wang [16], Holloway [17], Kang et al. [18], Niwa and Hibiya [19], Jan et al. [20], and Buijsman et al. [21] carried out many numerical studies on internal tides, which can be divided into two categories. One is the studies on generation mechanism and influence factors of internal tidal over an ideal topography, and the other is the studies on generation and propagation of internal tides in real oceans.

Determination of parameters is an important step in the numerical simulation of internal tides. As the most important parameter, the open boundary conditions have been studied very thoroughly [22–27]. But usually the open boundary conditions can be treated as being distributed in a line. On the other hand, the bottom friction coefficients (BFCs) with spatial distribution are also important coefficients in the study of tides. So far, however, the relevant studies are still very few. Chevalier et al. [28] carried out a regional study on the tidal hydrodynamics of the Hudson Bay with a finite element model T-UGOm. In the study, they prescribed the importance of regionally varying friction coefficients in computing energy budget. With a rapid development in computing technology and the progress of ocean observation technology, the adjoint method has been widely used in BFCs estimation. Das and Lardner [29, 30] estimated the spatially

varying BFCs and depth based on a 2D tidal model with the adjoint method. Ullman and Wilson [31] estimated the temporal and spatial variability of BFCs by assimilation data of ADCP in the Hudson River using the adjoint method. Heemink et al. [32] used the adjoint method to optimize open boundary conditions, spatially varying depth, and BFCs based on a 3D tidal model. Lu and Zhang [33] studied the inversion problem of spatially varying BFCs based on a 2D tidal model with the adjoint method and simulated the M_2 tide in the East China Sea. Zhang and Lu [34] constructed a three-dimensional numerical barotropic tidal model with the adjoint method and studied the estimation of the open boundary conditions, BFCs, and the vertical eddy viscosity coefficients based on their model. Zhang et al. [35] optimized the BFCs in the Bohai and Yellow Seas based on a 2D tidal model using the adjoint method. Altaf et al. [36] used the adjoint method to estimate the depth values and the BFCs in a large-scale shallow sea model. However, these studies did not involve how to determine BFCs in an internal tidal model. This paper is to present a train of thought to solve this problem.

Three groups of ideal experiments are performed to investigate the estimation of spatially varying BFCs based on an isopycnic-coordinate internal tidal model with the adjoint method. Group 1 investigates the influence that the distance between independent points (DIP) exerts on the inversion results. Group 2 investigates the influence of interpolation radius (IR) on the inversion results. And group 3 investigates the inversion problem of BFCs with 4 prescribed distributions. This paper is organized as follows. The isopycnic-coordinate internal tidal model with the adjoint method is briefly introduced in Section 2. Experimental design is presented in Section 3. Results are discussed in detail in Section 4. Finally, we make a summary and draw some conclusions in Section 5.

2. Model Introduction

In this paper, the isopycnic-coordinate internal tidal model with the adjoint method is the same as that constructed by Chen et al. [26], which contains a forward model and an adjoint one. The forward model is used to simulate internal tides and the adjoint one is used to optimize parameters using the adjoint method. The reasonability and feasibility of the model have been tested by Chen et al. [26]. And the formulation will not be detailed in this paper. In the following part, the derivation of BFCs adjustment and the independent point scheme are shown in detail.

2.1. BFCs Adjustment. According to the derivation of Chen et al. [26], we have the following first derivative of Lagrangian function with respect to BFC:

$$\frac{\partial L}{\partial \kappa_{i,j}} = 0, \tag{1}$$

where L is Lagrangian function and $\kappa_{i,j}$ is the value of BFC at grid (i, j). The gradient of cost function (i.e., J) with respect to $\kappa_{i,j}$ can be deduced by

$$\begin{aligned}\frac{\partial J}{\partial \kappa_{i,j}} = {} & \frac{\rho_l}{2}\sum_n \left[u^n_{i-1,j,l} u^n_{ai-1,j,l} \sqrt{\left(u^n_{i-1,j,l}\right)^2 + \left(\overline{v}^n_{i-1,j,l}\right)^2} \right. \\ & \left. + u^n_{i,j,l} u^n_{ai,j,l} \sqrt{\left(u^n_{i,j,l}\right)^2 + \left(\overline{v}^n_{i,j,l}\right)^2} \right] \\ & + \frac{\rho_l}{2}\sum_n \left[v^n_{i,j-1,l} v^n_{ai,j-1,l} \sqrt{\left(\overline{u}^n_{i,j-1,l}\right)^2 + \left(v^n_{i,j-1,l}\right)^2} \right. \\ & \left. + u^n_{i,j,l} u^n_{ai,j,l} \sqrt{\left(\overline{u}^n_{i,j,l}\right)^2 + \left(v^n_{i,j,l}\right)^2} \right],\end{aligned} \tag{2}$$

where ρ_l is the potential density in the lth layer, $u^n_{i,j,l}$ and $v^n_{i,j,l}$ are horizontal velocities at the nth time step, $u^n_{ai,j,l}$ and $v^n_{ai,j,l}$ are called the adjoint variables of $u^n_{i,j,l}$ and $v^n_{i,j,l}$, respectively, and $\overline{u}^n_{i,j,l}$ and $\overline{v}^n_{i,j,l}$ are values of the average over four digits, respectively.

Gradient descent method is used in deducing the adjustment formula of BFC. The adjustment formula is

$$\kappa^{m+1}_{i,j} = \kappa^m_{i,j} - \alpha \frac{\left(\partial J/\partial \kappa_{i,j}\right)^{(m)}}{\left\|\left(\partial J/\partial \kappa_{i,j}\right)^{(m)}\right\|}, \tag{3}$$

where α is the step length, $\kappa^m_{i,j}$ and $\kappa^{m+1}_{i,j}$ are the priori and adjusted values of BFC in the mth iteration, respectively, and $(\partial J/\partial \kappa_{i,j})^{(m)}$ is the gradient of cost function with respect to the BFC, whose L2-norm is $\|(\partial J/\partial \kappa_{i,j})^{(m)}\|$. In order to guarantee that the cost function declines steadily, formula (3) could be modified as follows:

$$\kappa^{m+1}_{i,j} = \kappa^m_{i,j} - \alpha \frac{\left\|\left(\partial J/\partial \kappa_{i,j}\right)^{(m)}\right\|}{\left\|\left(\partial J/\partial \kappa_{i,j}\right)^{(1)}\right\|} \cdot \frac{\left(\partial J/\partial \kappa_{i,j}\right)^{(m)}}{\left\|\left(\partial J/\partial \kappa_{i,j}\right)^{(m)}\right\|}. \tag{4}$$

2.2. Independent Point Scheme. Considering that the amount of available observations is limited in practical applications, the independent point scheme, which is easy to implement mathematically and reasonable physically, is employed in parameter optimization. A proper independent point scheme can improve the accuracy of parameter estimation, so as to improve the accuracy of simulation results [37].

The basic idea of optimizing BFCs with independent point scheme is described as follows. Some grids in computational area are selected as independent points. Values of BFCs at independent points are obtained by using adjoint method and those at other grids are obtained by interpolation, which can be described as follows:

$$\kappa_{i,j} = \frac{\sum_{ii,jj} W_{i,j,ii,jj}\, \kappa_{ii.jj}}{\sum_{ii,jj} W_{i,j,ii,jj}}, \tag{5}$$

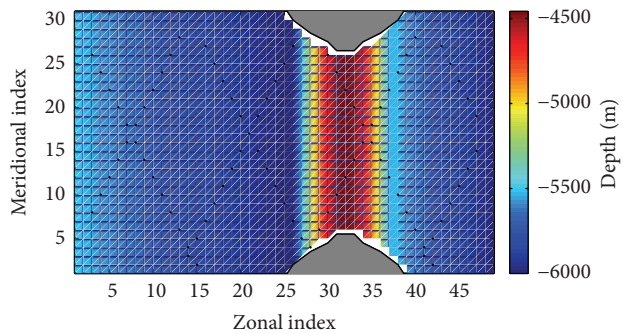

Figure 1: Plan view of calculation region (black dots are observation locations).

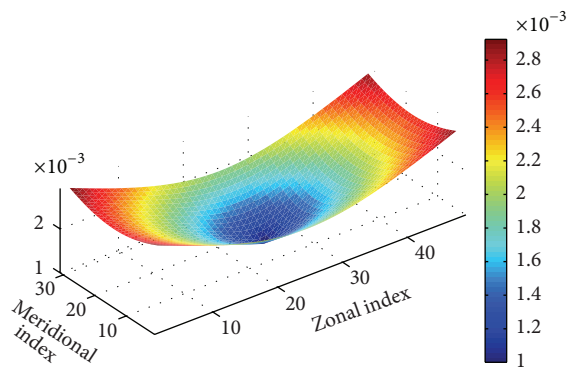

Figure 2: The prescribed BFCs with distribution of conical surface.

where $\kappa_{ii,jj}$ is the value of BFC at independent point (ii, jj), $\kappa_{i,j}$ is the value at other grids (i, j), and $W_{i,j,ii,jj}$ is the weight coefficient, which adopts the form of Cressman [38]:

$$W_{i,j,ii,jj} = \frac{R^2 - r_{i,j,ii,jj}^2}{R^2 + r_{i,j,ii,jj}^2}, \tag{6}$$

where $r_{i,j,ii,jj}$ is the distance between (i, j) and (ii, jj) and R is the interpolation radius. Then the gradient of cost function with respect to $\kappa_{ii,jj}$ is computed as

$$\frac{\partial J}{\partial \kappa_{ii,jj}} = \frac{\sum_{i,j} W_{i,j,ii,jj} \left(\partial J / \partial \kappa_{i,j}\right)}{\sum_{i,j} W_{i,j,ii,jj}}, \tag{7}$$

where $\partial J / \partial \kappa_{i,j}$ is the gradient of cost function with respect to $\kappa_{i,j}$, which is calculated by (2).

3. Experimental Design

The calculation region (from 116°E to 124°E and from 18°E to23°E) with an ideal topography is shown in Figure 1. The horizontal resolution in this model is $10' \times 10'$ and there are 49×31 grids totally in this area. The initial undisturbed interface of this model is placed at the depth of 200 m, and the potential densities in two layers are 1023.42 kg/m^3 and 1025.90 kg/m^3, respectively, based on the temperature-salinity data of the world oceans data sets (WOA05). The Coriolis parameter is equal to the local value, the angular frequency of M_2 tide is $1.4050789025 \times 10^{-4} s^{-1}$, and the time step is 496.863 s (i.e., 1/90 of the period of M_2 tide) for both external and internal modes. The time of simulation is equal to 20 periods of M_2 tide. The horizontal eddy viscosity coefficient (A_h) and interface friction coefficient (A_v) are equal to 1000 m^2/s and 0.02 m^2/s, respectively. The step length is 0.001. The Flather conditions are installed along four boundaries and, without loss of generality, the unknown open boundary is supposed to be east boundary. Based on the distribution characteristics of the TEPOX/Poseidon (T/P) satellite altimeter, some points under T/P tracks are selected as observation locations. Every observation location has "observations" of interface elevation.

Based on the model, three groups of ideal experiments (i.e., groups 1 to 3) are carried out to investigate the estimation of the spatially varying BFCs. In all groups, values of the prescribed BFC range from 1×10^{-3} m^2/s to 3×10^{-3} m^2/s. In groups 1 and 2, BFCs with the distribution of conical surface are prescribed and shown in Figure 2. In group 3, BFCs with 4 distributions are prescribed and shown in Figure 3.

In group 1, five strategies are implemented to investigate the influence that the DIP exerts on the inversion results. The DIPs are $30'$, $40'$, $50'$, $60'$, and $70'$, and the IR are $60'$, $80'$, $100'$, $120'$, and $140'$ corresponding to 5 strategies, respectively. That is to say, the IR is 2 times of DIP in this group.

In group 2, the optimal DIP in group 1 is employed, and 5 strategies are implemented to investigate the influence of IR

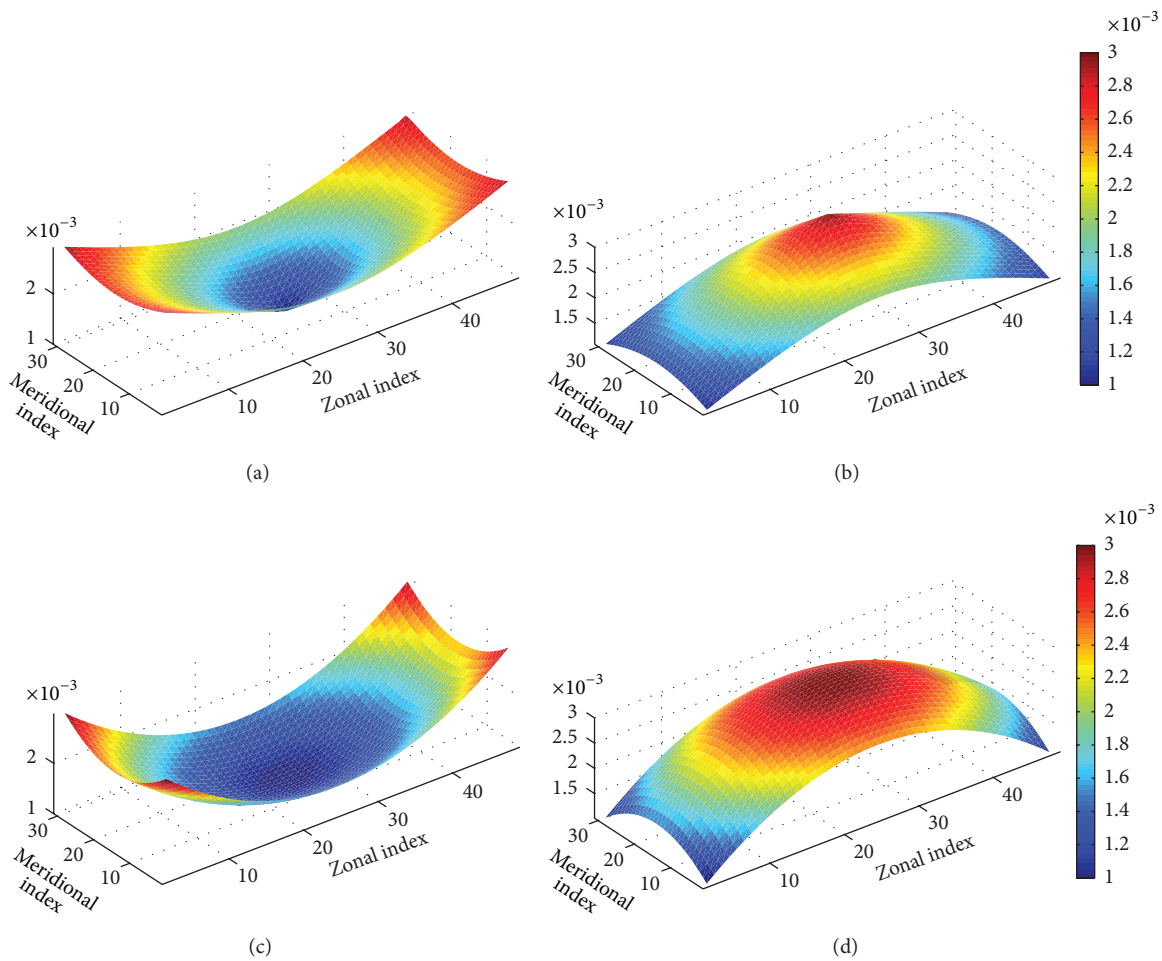

Figure 3: Four prescribed distributions of BFCs.

on the inversion results. The interpolation radii corresponding to 5 strategies are 1.7, 1.8, 1.9, 2.0, and 2.1 times of DIP, respectively.

In group 3, the optimal DIP and IR obtained based on the results of the previous experiments are employed to invert the BFCs with 4 prescribed distributions. The prescribed distributions are shown in Figure 3, in which panels (a) and (b) are two conical surfaces, while panels (c) and (d) are two paraboloids of revolution.

4. Experimental Results and Discussions

In the process of parameter optimization, different iteration numbers are tried in group 1, and 100 iterations are a good choice based on the following considerations: (1) the misfit between "observations" and the simulated results is very small and approximately constant when it declines to a certain value after 100 iterations; (2) the cost functions are almost no longer falling after 100 iterations; (3) the calculation amount is acceptable for the 100 iterations. In the other two groups, the iteration number is also taken as 100.

Table 1: Statistics of the REs of inversion results obtained with 5 strategies.

Strategies	1	2	3	4	5
Ratio (RE < 10%)	77.4%	86.0%	87.8%	87.5%	84.8%
Ratio (RE > 20%)	5.9%	2.7%	2.7%	2.4%	2.8%

4.1. Results and Discussions of Group 1. The DIPs in 5 strategies in group 1 are $30'$, $40'$, $50'$, $60'$, and $70'$, respectively. The prescribed and inverted distributions of BFCs are shown in Figure 4 and the mean absolute errors (MAEs) between them are shown in Figure 5. From Figure 4 we can find that all the inverted distributions show good agreements with the prescribed one, indicating that, by using independent point scheme, the BFCs with the distribution of conical surface can be inverted successfully. The MAE in BFCs before assimilation is 3.67×10^{-4}. After assimilation, all the MAEs are decreased especially for Strategy 3, of which the value reaches the minimum in this group.

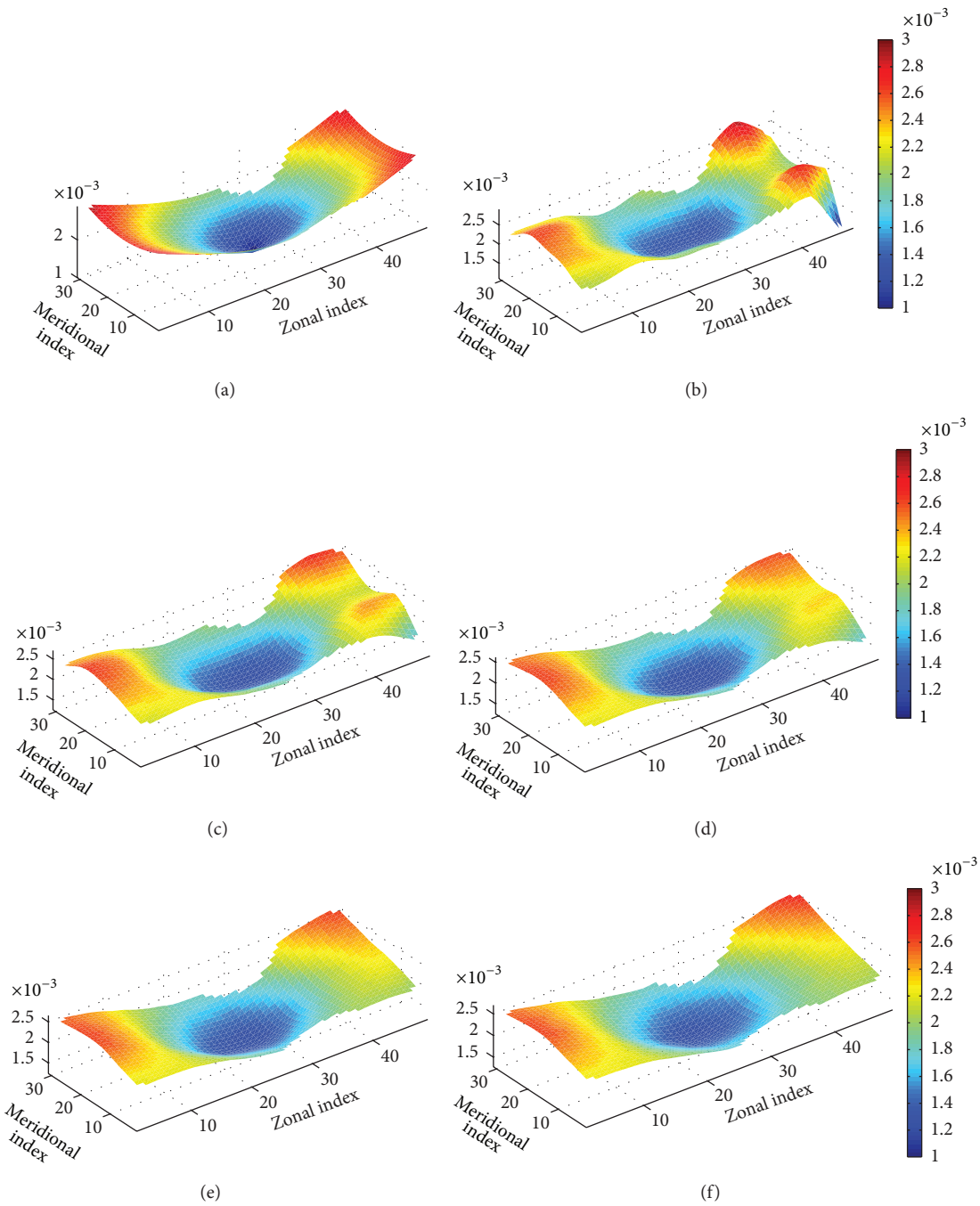

Figure 4: The prescribed and inverted distributions of BFCs obtained with 5 strategies.

Table 2: The AVDs in interface elevation obtained with 5 strategies (AA indicates after assimilation, BA indicates before assimilation).

Strategies	AA (10^{-5} m)	1−AA/BA (%)
1	11.14	84.5
2	8.81	87.7
3	8.28	88.5
4	7.90	89.0
5	8.65	87.9

Statistics of the relative errors (REs) of inversion results and average vector differences (AVDs) between pseudoobservations and simulated results are listed in Tables 1 and 2, respectively. At most grids, the REs are less than 10%, while only at very few grids, the values are more than 20%, suggesting the feasibility of the model. The AVD in interface elevation before assimilation is 7.17×10^{-4}. From Table 2 we can find that, after assimilation, the AVDs are decreased dramatically compared with the value before assimilation.

The iteration histories of the cost functions and their gradient norms with respect to BFCs (all values are normalized

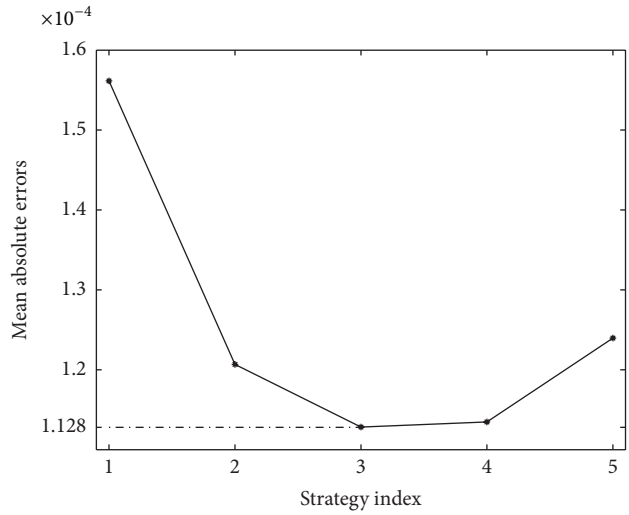

Figure 5: The MAEs in BFCs obtained with 5 strategies.

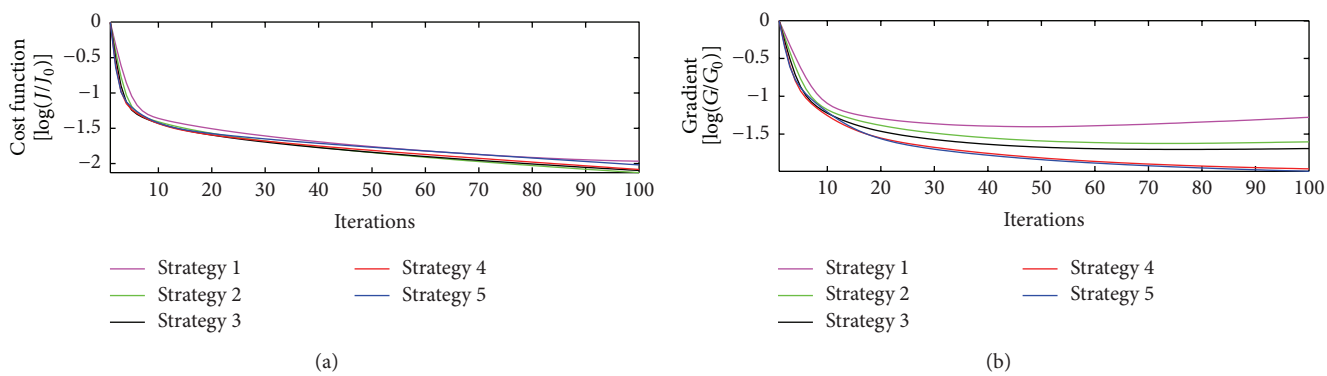

Figure 6: The iteration histories of the cost functions and their gradient norms obtained with 5 strategies (J_0 and G_0 are the values of cost function and its gradient norm before assimilation, resp.).

by their own initial values) are shown in Figure 6. The cost functions and their gradient norms are declining dramatically during the assimilation process. After 100 iterations, the cost functions and their gradient norms are reduced by more than 2 orders of magnitude and by more than 1 order of magnitude compared with their initial values, respectively, implying the efficiency of the gradient descent method.

Based on the above analysis, the following conclusions can be summarized: the BFCs with the distribution of conical surface can be inverted successfully based on the isopycnic-coordinate internal tidal model with the adjoint method; The use of a proper DIP can indeed effectively improve the precision of parameter estimation, and the DIP of $50'$ can lead to the best inversion results.

4.2. Results and Discussions of Group 2. According to the conclusion in Section 4.1, the DIP in this group is set to be $50'$. And 5 strategies are implemented to investigate the influence of IR on the inversion results. The interpolation radii in 5 strategies are 1.7, 1.8, 1.9, 2.0, and 2.1 times of DIP, respectively. The prescribed and inverted distributions of BFCs are shown in Figure 7 and the MAEs between them are shown in Figure 8. From Figure 7 we can find that all the inverted distributions show good agreements with the prescribed one. The MAE in BFCs before assimilation is 3.67×10^{-4}. After assimilation, all the MAEs are decreased especially for Strategy 3, of which the value reaches the minimum.

In addition, numerical experimental results show that, after 100 iterations, the cost functions and their gradient norms are reduced by more than 2 orders of magnitude and by more than 1 order of magnitude compared with their initial values, respectively.

Based on the above analysis, the use of a proper IR can indeed effectively improve the precision of parameter estimation, and the IR of 1.9 times of DIP can lead to the best inversion results.

For the BFCs with the distribution of conical surface, the DIP is set to be $50'$ and the IR is set to be 1.9 times of DIP which leads to the best inversion results.

4.3. Results and Discussions of Group 3. Based on the results of the first two groups of experiments, the DIP is set to be $50'$ and the IR is set to be 1.9 times of DIP in this group. Four

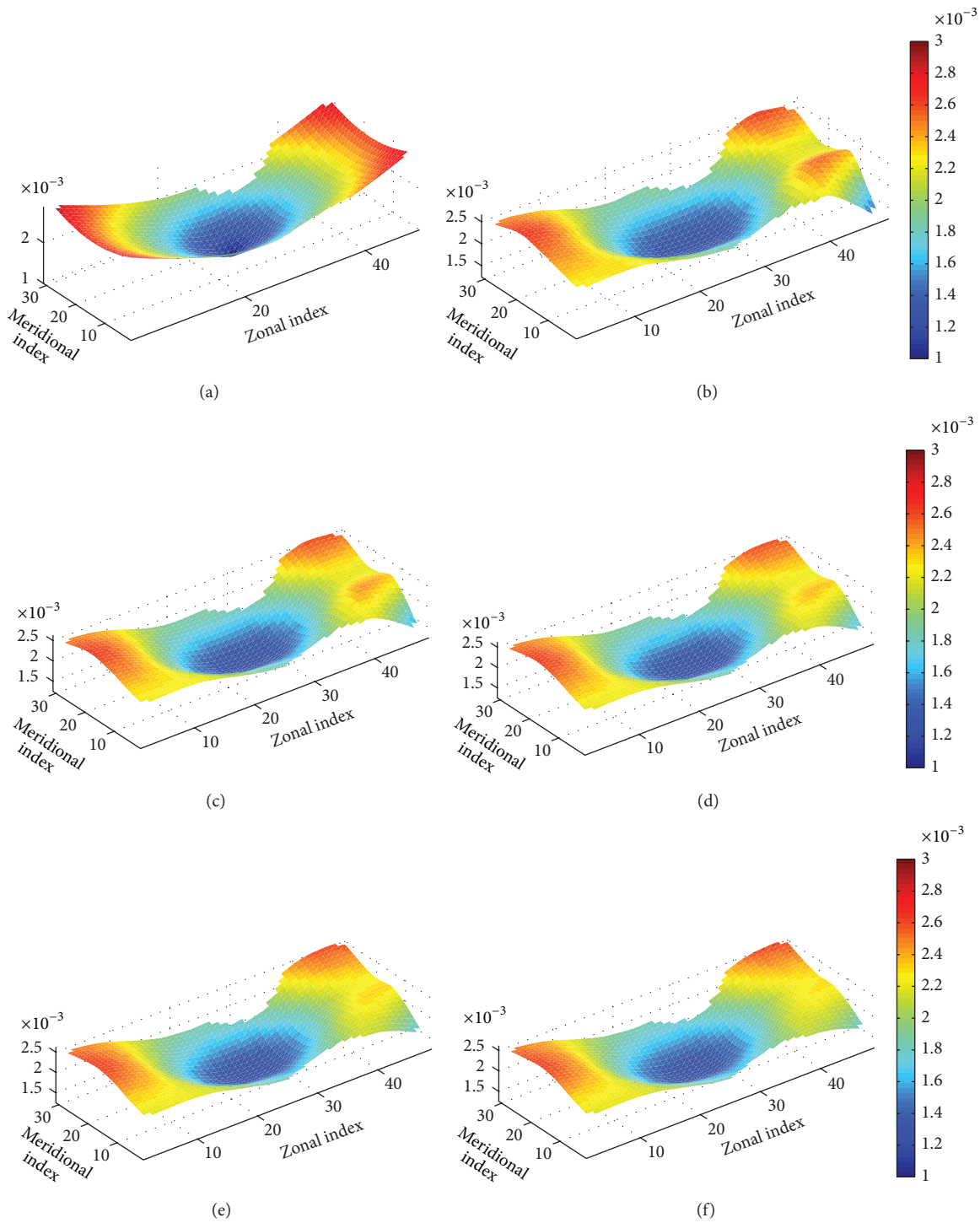

Figure 7: The prescribed and inverted distributions of BFCs obtained with 5 strategies.

experiments are carried out to invert 4 distributions of BFCs. The inverted distributions of BFCs are shown in Figure 9. From Figure 9 we can find that all the inverted distributions show good agreements with the prescribed ones, indicating that all 4 prescribed distributions of BFCs can be inverted successfully.

The MAEs in BFCs before and after assimilation are listed in Table 3, which shows that the MAEs after assimilation are decreased compared with the values before assimilation; the MAEs after assimilation with the distributions of two conical surfaces exceed those with the distributions of two revolution paraboloids.

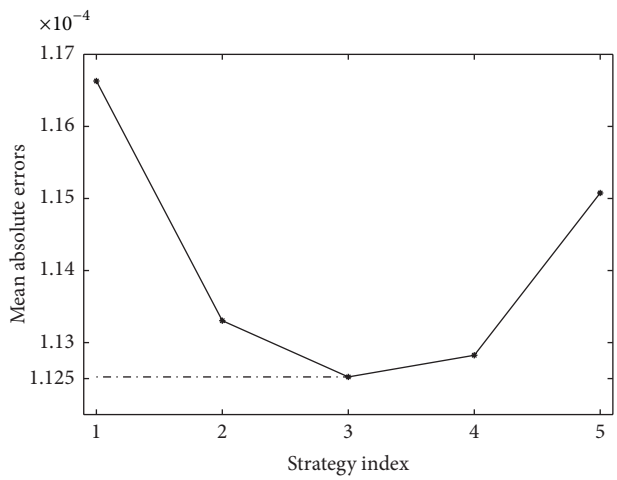

Figure 8: The MAEs in BFCs with 5 strategies.

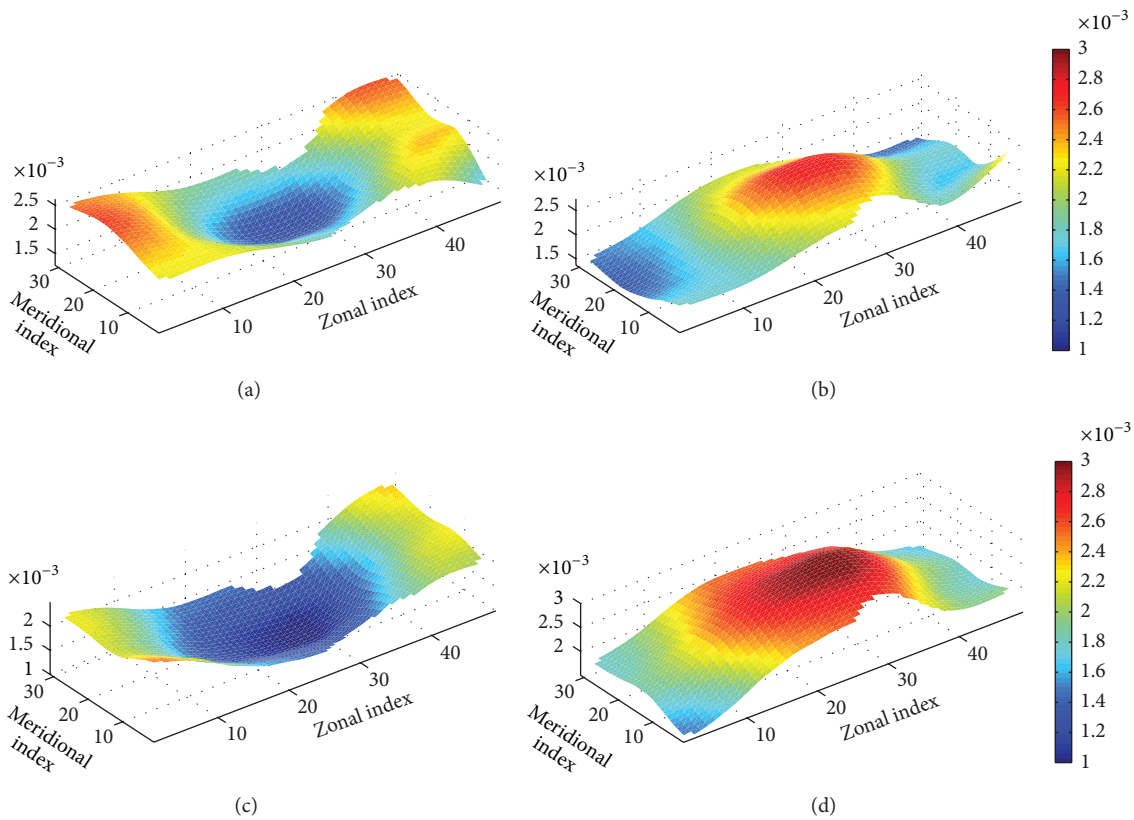

Figure 9: The 4 inverted distributions of BFCs.

The iteration histories of the cost functions and their gradient norms (all values are normalized by their own initial values) are shown in Figure 10, which shows that the cost functions and their gradient norms are declining dramatically during the assimilation process; after 100 iterations, the cost functions and their gradient norms are reduced by more than 2 orders of magnitude and by more than 1 order of magnitude compared with their initial values, respectively; the descent of the two indexes (i.e., the cost functions and their gradient norms) for the two revolution paraboloids are superior to those for the two conical surfaces.

Based on the above analysis, the isopycnic-coordinate internal tidal model with the adjoint method has a good ability in estimating the spatially varying BFCs, and the inversion results of the BFCs with the distribution of revolution paraboloid are better than those with the distribution

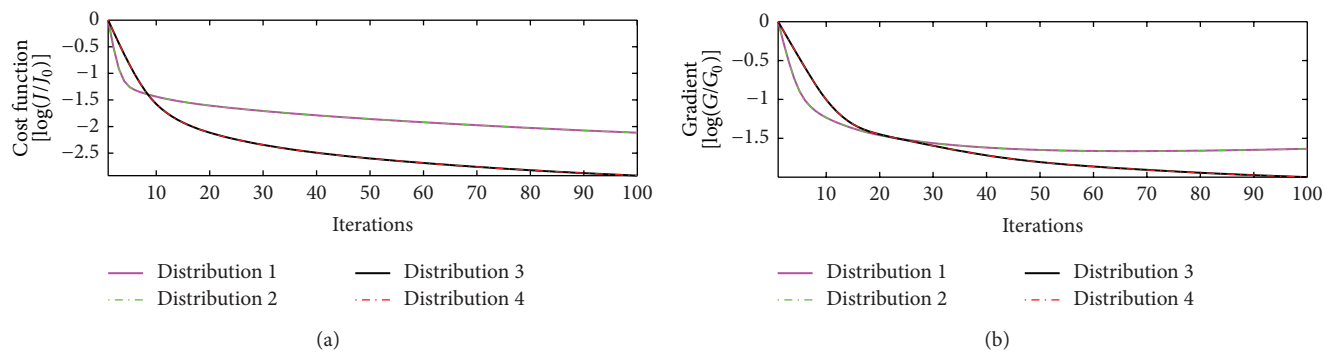

Figure 10: The iteration histories of the cost functions and their gradient norms (J_0 and G_0 are the values of cost function and its gradient norm before assimilation, resp.).

of conical surface. We think that the prescribed BFCs with the distribution of conical surface change more remarkably than those with the distribution of revolution paraboloid; The prescribed BFCs with the distribution of conical surface have a cuspidal point, while those with the distribution of revolution paraboloid do not.

Table 3: The MAEs in BFCs before assimilation (BA) and after assimilation (AA).

Distributions	1	2	3	4
BA ($\times 10^{-4}$)	3.7	3.7	5.0	5.0
AA ($\times 10^{-4}$)	1.1	1.1	1.0	1.0
1−AA/BA (%)	70.3	70.3	80.0	80.0

5. Summary and Conclusions

Based on the isopycnic-coordinate internal tidal model with the adjoint method, three groups of ideal experiments are carried out in order to investigate the estimation of spatially varying BFCs.

In group 1, five strategies are implemented to investigate the influence that the DIP exerts on the inversion results. The numerical experimental results show that by using independent point scheme, the BFCs with the distribution of conical surface can be inverted successfully; the MAEs in BFCs after assimilation are decreased compared with the value before assimilation, and especially, the MAE obtained with the strategy with a DIP of $50'$ reaches the minimum; The cost functions and their gradient norms with respect to BFCs are declining dramatically during the assimilation process. The numerical experimental results indicate that the strategy with a DIP of $50'$ leads to the best inversion results.

In Group 2, the DIP is set to be $50'$, and 5 strategies are implemented to investigate the influence of IR on the inversion results. The numerical experimental results show that the MAEs after assimilation are decreased compared with the value before assimilation, and, especially, the MAE obtained with the strategy with an IR of 1.9 times of DIP reaches the minimum; after assimilation, the cost functions and their gradient norms are all reduced dramatically. The numerical experimental results indicate that the strategy with an IR of 1.9 times of DIP leads to the best inversion results.

In group 3, the DIP is set to be $50'$ and the IR is set to be 1.9 times of DIP based on the results of the first two groups of experiments. Four experiments are carried out to invert 4 distributions of BFCs, respectively. The numerical experimental results show that all 4 prescribed distributions of BFCs are inverted successfully; the MAEs after assimilation are decreased compared with the value before assimilation, and furthermore the MAEs with the distributions of two conical surfaces exceed those with the distributions of two revolution paraboloids; after 100 iterations, the cost functions and their gradient norms are all reduced dramatically, and the cost functions and their gradient norms with the two conical surfaces are superior to those with the two revolution paraboloids. The numerical experimental results indicate that the isopycnic-coordinate internal tidal model with the adjoint method has a good ability in estimating the spatially varying BFCs, and the inversion results of BFCs with the distribution of revolution paraboloid are better than those with the distribution of conical surface.

The ideal experiments successfully invert the spatially varying BFCs based on the isopycnic-coordinate internal tidal model with the adjoint method. The optimal independent point scheme can be used as a reference for numerical simulation of internal tides in the South China Sea. The work in this paper provides a way for parameter optimization in study of internal tide. For the spatially varying coefficients of the interface friction and the horizontal eddy viscosity, we can borrow this way to determine the values in internal tide simulation.

Acknowledgments

The authors acknowledge the support of the Major State Basic Research Development Program of China through Grant 2013CB956500, the National Natural Science Foundation of China through Grants 41072176 and 41206001, the Natural Science Foundation of Jiangsu Province of China through Grant BK2012315, and the Fundamental Research Funds for the Central Universities 201261006 and 201262007.

References

[1] P. G. Baines, "On internal tide generation models," *Deep Sea Research A*, vol. 29, no. 3, pp. 307–338, 1982.

[2] K. E. Gustafsson, "Computations of the energy flux to mixing processes via baroclinic wave drag on barotropic tides," *Deep Sea Research I*, vol. 48, no. 10, pp. 2283–2295, 2001.

[3] H. L. Simmons, R. W. Hallberg, and B. K. Arbic, "Internal wave generation in a global baroclinic tide model," *Deep Sea Research II*, vol. 51, no. 25-26, pp. 3043–3068, 2004.

[4] W. Munk and C. Wunsch, "Abyssal recipes II: energetics of tidal and wind mixing," *Deep Sea Research I*, vol. 45, no. 12, pp. 1977–2010, 1998.

[5] G. D. Egbert and R. D. Ray, "Significant dissipation of tidal energy in the deep ocean inferred from satellite altimeter data," *Nature*, vol. 405, no. 6788, pp. 775–778, 2000.

[6] Y. Niwa and T. Hibiya, "Numerical study of the spatial distribution of the M_2 internal tide in the Pacific Ocean," *Journal of Geophysical Research C*, vol. 106, no. 10, pp. 22441–22449, 2001.

[7] D. L. Rudnick, T. J. Boyd, R. E. Brainard et al., "From tides to mixing along the Hawaiian Ridge," *Science*, vol. 301, no. 5631, pp. 355–357, 2003.

[8] J. Tian, L. Zhou, and X. Zhang, "Latitudinal distribution of mixing rate caused by the M_2 internal tide," *Journal of Physical Oceanography*, vol. 36, no. 1, pp. 35–42, 2006.

[9] M. Rattray Jr., "On the coastal generation of internal tides," *Tellus*, vol. 12, pp. 54–62, 1960.

[10] P. G. Baines, "The generation of internal tides by flat-bump topography," *Deep Sea Research and Oceanographic Abstracts*, vol. 20, no. 2, pp. 179–205, 1973.

[11] P. G. Baines, "On internal tide generation models," *Deep Sea Research A*, vol. 29, no. 3, pp. 307–338, 1982.

[12] T. Gerkema, "A unified model for the generation and fission of internal tides in a rotating ocean," *Journal of Marine Research*, vol. 54, no. 3, pp. 421–450, 1996.

[13] C. Garrett and T. Gerkema, "On the body-force term in internal-tide generation," *Journal of Physical Oceanography*, vol. 37, no. 8, pp. 2172–2175, 2007.

[14] S. G. Llewellyn Smith and W. R. Young, "Conversion of the barotropic tide," *Journal of Physical Oceanography*, vol. 32, no. 5, pp. 1554–1566, 2002.

[15] N. J. Balmforth and T. Peacock, "Tidal conversion by supercritical topography," *Journal of Physical Oceanography*, vol. 39, no. 8, pp. 1965–1974, 2009.

[16] W. S. Chuang and D. P. Wang, "Effects of density front on the generation and propagation of internal tides," *Journal of Physical Oceanography*, vol. 11, no. 10, pp. 1357–1374, 1981.

[17] P. E. Holloway, "A numerical model of internal tides with application to the Australian North West Shelf," *Journal of Physical Oceanography*, vol. 26, no. 1, pp. 21–37, 1996.

[18] S. K. Kang, M. G. G. Foreman, W. R. Crawford, and J. Y. Cherniawsky, "Numerical modeling of internal tide generation along the Hawaiian Ridge," *Journal of Physical Oceanography*, vol. 30, no. 5, pp. 1083–1098, 2000.

[19] Y. Niwa and T. Hibiya, "Three-dimensional numerical simulation of M_2 internal tides in the East China Sea," *Journal of Geophysical Research C*, vol. 109, no. 4, Article ID C04027, 2004.

[20] S. Jan, C.-S. Chern, J. Wang, and S.-Y. Chao, "Generation of diurnal K_1 internal tide in the Luzon Strait and its influence on surface tide in the South China Sea," *Journal of Geophysical Research C*, vol. 112, no. 6, Article ID C06019, 2007.

[21] M. C. Buijsman, Y. Uchiyama, J. C. Mcwilliams, and C. R. Hill-Lindsay, "Modeling semidiurnal internal tide variability in the southern california bight," *Journal of Physical Oceanography*, vol. 42, no. 1, pp. 62–77, 2012.

[22] R. W. Lardner, "Optimal control of open boundary conditions for a numerical tidal model," *Computer Methods in Applied Mechanics and Engineering*, vol. 102, no. 3, pp. 367–387, 1993.

[23] I. Shulman, J. K. Lewis, A. F. Blumberg, and B. N. Kim, "Optimized boundary conditions and data assimilation with application to the M_2 tide in the yellow sea," *Journal of Atmospheric and Oceanic Technology*, vol. 15, no. 4, pp. 1066–1071, 1998.

[24] A. Zhang, E. Wei, and B. B. Parker, "Optimal estimation of tidal open boundary conditions using predicted tides and adjoint data assimilation technique," *Continental Shelf Research*, vol. 23, no. 11–13, pp. 1055–1070, 2003.

[25] J. Nycander, A. M. Hogg, and L. M. Frankcombe, "Open boundary conditions for nonlinear channel flow," *Ocean Modelling*, vol. 24, no. 3-4, pp. 108–121, 2008.

[26] H. Chen, C. Miao, and X. Lv, "A three-dimensional numerical internal tidal model involving adjoint method," *International Journal for Numerical Methods in Fluids*, vol. 69, no. 10, pp. 1584–1613, 2012.

[27] Y. Gao, G. Jin, H. Chen, and X. Lv, "Estimation of open boundary conditions based on an isopycnic-coordinate internal tidal model with adjoint assimilation method," *Mathematical Problems in Engineering*, vol. 2013, Article ID 321387, 11 pages, 2013.

[28] L. Chevalier, F. Lyard, D. Greenberg, and Y. Soufflet, "Tidal hydrodynamics of the Hudson Bay and its impact in the global ocean tide," in *Proceedings of the EGU General Assembly Conference Abstracts*, vol. 15, p. 1132, Vienna, Austria, April 2013.

[29] S. K. Das and R. W. Lardner, "On the estimation of parameters of hydraulic models by assimilation of periodic tidal data," *Journal of Geophysical Research*, vol. 96, no. 8, pp. 15187–15196, 1991.

[30] S. K. Das and R. W. Lardner, "Variational parameter estimation for a two-dimensional numerical tidal model," *International Journal for Numerical Methods in Fluids*, vol. 15, no. 3, pp. 313–327, 1992.

[31] D. S. Ullman and R. E. Wilson, "Model parameter estimation from data assimilation modeling: temporal and spatial variability of the bottom drag coefficient," *Journal of Geophysical Research C*, vol. 103, no. 3, pp. 5531–5549, 1998.

[32] A. W. Heemink, E. E. A. Mouthaan, M. R. T. Roest, E. A. H. Vollebregt, K. B. Robaczewska, and M. Verlaan, "Inverse 3D shallow water flow modelling of the continental shelf," *Continental Shelf Research*, vol. 22, no. 3, pp. 465–484, 2002.

[33] X. Lu and J. Zhang, "Numerical study on spatially varying bottom friction coefficient of a 2D tidal model with adjoint method," *Continental Shelf Research*, vol. 26, no. 16, pp. 1905–1923, 2006.

[34] J. Zhang and X. Lu, "Parameter estimation for a three-dimensional numerical barotropic tidal model with adjoint method," *International Journal for Numerical Methods in Fluids*, vol. 57, no. 1, pp. 47–92, 2008.

[35] J. Zhang, X. Lu, P. Wang, and Y. P. Wang, "Study on linear and nonlinear bottom friction parameterizations for regional tidal models using data assimilation," *Continental Shelf Research*, vol. 31, no. 6, pp. 555–573, 2011.

[36] M. U. Altaf, M. Verlaan, and A. W. Heemink, "Efficient identification of uncertain parameters in a large-scale tidal model

of the European continental shelf by proper orthogonal decomposition," *International Journal for Numerical Methods in Fluids*, vol. 68, no. 4, pp. 422–450, 2012.

[37] J. Zhang and X. Lu, "On the simulation of M_2 tide in the Bohai, Yellow, and East China Seas with TOPEX/Poseidon altimeter data," *Terrestrial, Atmospheric and Oceanic Sciences*, vol. 19, no. 1-2, pp. 173–181, 2008.

[38] G. P. Cressman, "An operational objective analysis system," *Monthly Weather Review*, vol. 87, pp. 367–374, 1959.